Calorimeter Response Deconvolution for Energy Estimation in High-Luminosity Conditions

Luciano M. de A. Filho, Bernardo S. Peralva, José M. de Seixas, and Augusto S. Cerqueira

***Abstract*—Signal superposition, also called pile-up noise, has become an important issue for calorimeters operating under high-luminosity conditions. Current techniques model those superimposed signals as highly correlated noise, whose covariance matrix information is used to develop a minimal variance and unbiased filter for energy estimation. Hence, the filter coefficients depend on the current luminosity. This paper presents a new energy estimator whose design is independent of the luminosity. The method consists of deconvolving the front-end electronic shaping response, recovering the primary impulse signals. The deconvolution process allows the identification of each superimposed component. Based on that information, it is possible to include additional constraints in order to design orthogonal estimators for each component, providing optimal estimators suitable to operate in colliders where luminosity changes during the run. Comparisons between current approaches and the proposed method using pile-up event simulation are presented. Results point out that an improvement on amplitude estimation performance is achieved and stable signal reconstruction is provided for different luminosity ranges.**

***Index Terms*—Amplitude estimators, calorimetry, energy reconstruction, linear deconvolution.**

I. Introduction

POWERFUL high-energy machines are built to collide particle beams up to a rate of the order of tens of millions of collisions per second. These machines tend to increase their collision rates and the number of particles in a bunch aiming at providing a higher probability to observe rare physics processes [1], [2]. By increasing the number of interactions per Bunch-Crossing (BC), a larger amount of signals becomes available for analysis, which improves statistical significance. However, the high-luminosity scenario brings new challenges in terms of data acquisition and signal processing.

Calorimeters play an important role in modern high-energy experiments [3]. Typically, calorimeters have thousands of readout channels whose signals depend on the specific calorimeter principle and signal shaping. The particle energy is sampled and its value is proportional to the acquired electronic pulse amplitude, whose shaping is considered to be fixed for the entire dynamic range.

Energy reconstruction is typically carried out by performing a weighted sum of digitized pulse samples, in order to minimize the noise contribution on the pulse amplitude estimation. The front-end analog-to-digital converter (ADC) sampling frequency is synchronized with the experiment event rate so that each collision subproduct is assigned to a given BC identification (BCID) number. A constant pedestal value is generally added to the analog signal before its digitization, in order to avoid negative ADC conversion values. There is also a pulse phase shift, which is a random variable that can be modelled as a zero-mean uniform distribution bounded by an absolute value smaller than the ADC sampling period. Different times of flight and particle paths produce pulses that can have a time shift with respect to in-time particles. In some cases, such a phase shift can be neglected.

Usually, readout signals are unipolar [4]–[7] and can be spread along several adjacent BCs, suffering from out-of-time (OOT) signal superposition in high-luminosity conditions. This signal overlapping, commonly called "pile-up", degrades the original pulse shaping, compromising the performance of the energy estimation task. The classical approach to deal with the pile-up was proposed in [8] and has been used so far in modern collider detectors [9]–[11]. The method considers the pile-up effect as an additive noise source that is handled through the use of the background second-order statistics information. The amplitude estimator method uses the resulting noise covariance matrix in a whitening process, which is intrinsic to a linear filter design procedure based on variance minimization [12]. Hence, the amplitude estimator remains optimal only for Gaussian noise. However, depending on the reference pulse-shape, the pile-up effect adds positive or negative tails to the noise distribution, which becomes non-Gaussian. Besides, that stochasticity is nonstationary, since the covariance matrix will change as a function of the number of primary collisions along a specific run.

In this paper, instead of combining the incoming pulse samples focusing on the amplitude estimation of the central signal, a deconvolution process is used to recover the original impulse signals generated at each BC. Deconvolution techniques have largely been used in digital signal processing for communication channel equalization [13], among other applications. The received signal can be modeled as a convolution between the target signal and the transmission channel response. An inversion filter at the receiver end, tuned to cancel the channel response, performs the deconvolution process and the target signal

Manuscript received March 09, 2015; revised July 18, 2015; accepted August 27, 2015. Date of publication November 09, 2015; date of current version December 11, 2015. This work was supported in part by CAPES, in part by CNPq, in part by FAPERJ, in part by FAPEMIG and the National Network for High Energy Physics (RENAFAE) in Brazil, and in part by the European Union (E-Planet Project).

L. M. de A. Filho, B. S.-M. Peralva, and A. S. Cerqueira are with the Electrical Engineering department of the Federal University of Juiz de Fora (UFJF), Juiz de Fora 36036-900, Brazil.

J. M. de Seixas is with the Electrical Engineering Department of the Federal University of Rio de Janeiro (COPPE/UFRJ), Rio de Janeiro 21945-970, Brazil.

Color versions of one or more of the figures in this paper are available online at http://ieeexplore.ieee.org.

Digital Object Identifier 10.1109/TNS.2015.2481714

can be fully recovered. The entire calorimeter signal production chain is interpreted here as a linear system whose response must be compensated for by using a deconvolution process. It opens a new perspective for applying modern digital-signal-processing methods in calorimetry.

In applying the deconvolution process, an uninterrupted data stream (commonly known as free-running) is necessary. For its use on the proposed scenario though, where only short acquisition window samples (few BCs) are available, the deconvolution procedure cannot be fully accomplished. This paper proposes an optimal approximation for the deconvolution process when only a few samples of the channel response are available. The method is based on mean square error (MSE) minimization and its relationship with optimal amplitude estimators is presented as well.

The target signal recovering strategy proposed here aims to be luminosity independent and enables simultaneous energy reconstruction of several adjacent BCs. The information from the neighboring BCs can be used to improve the final energy reconstruction procedure [14], [15]. After deconvolution, the BCs with signals are identified and their respective amplitudes can be fine tuned by using optimal amplitude estimators on the BCs where signals were detected. This procedure comprises the design of an amplitude estimator vector whose components are orthogonal to each other.

This multiamplitude estimation procedure allows confident signal pulse-shape reconstruction even under severe pile-up conditions. It allows classifying good quality reconstructed events against noisy and corrupted/saturated signals. The reconstruction error (RE) measure is typically computed from the squared root of MSE between the received samples and estimated signal [16], [17]. If the pulse shape can be considered invariant, this information can be used to reconstruct the analog front-end signals and the difference between the samples and the reconstructed pulse shape can be used as a performance measure. The multiple amplitude estimation characteristic of the proposed method allows such pulse-shape reconstruction quality evaluation even under pile-up, since the OOT signals are also used to recover the original signal.

This paper is organized as follows. The next section provides a brief explanation of the current amplitude estimation techniques used in modern calorimeter systems. Section III presents the theory behind the proposed method. Section IV covers the deconvolution algorithm implementation. Simulation results showing the performance of the proposed deconvolution approach are given in Section V. Section VI shows how to use the deconvolution process in the design of optimal vector estimators, and how this vector can be used to measure the goodness of the signal reconstruction under pile-up conditions. The estimation efficiency for different calorimeter pulse shapes, operating under different occupancy scenarios and signal to pile-up ratio levels, is also outlined at the end of Section VI. Finally, conclusions are derived in Section VII.

II. Optimal Amplitude Estimators

The energy reconstruction strategy in modern calorimeter systems consists of estimating the pulse amplitude through some optimization procedures. In high-event rate experiments, the amplitude estimation must be carried out fast, typically by a finite impulse response (FIR) filter [18]. The best linear unbiased estimator (BLUE) [12] is the most suitable method for online energy reconstruction, as it provides a linear, simple, and fast operation through a weighted sum of the incoming samples. Thus, although different optimization criteria are currently employed, linearity is a common constraint and the methods converge to the BLUE design.

Providing that a system can be modeled as a linear combination of the form

$$\mathbf{y} = \mathbf{U}\boldsymbol{\theta} + \mathbf{w} \tag{1}$$

where $\mathbf{y}$ is a vector corresponding to the observed samples (e.g., calorimeter readout), $\mathbf{U}$ is a matrix whose columns represent the superimposed reference patterns (e.g., shifted calorimeter pulse shape), and $\mathbf{w}$ is a zero-mean additive noise, the BLUE solution for the vector parameter bf $\boldsymbol{\theta}$ (e.g., signal amplitude) is given by [12]

$$\hat{\boldsymbol{\theta}} = (\mathbf{U}'\mathbf{C}^{-1}\mathbf{U})^{-1}\mathbf{U}'\mathbf{C}^{-1}\mathbf{y}. \tag{2}$$

In this equation, $\mathbf{C}$ is the noise covariance matrix and the single prime superscript character denotes the matrix transposition operator.

In order to apply the BLUE method in the calorimeter signal reconstruction problem, a linear model for the observed samples must be developed. Equation (3) shows a model often used [10]

$$\begin{bmatrix} y[1] \\ \vdots \\ y[N] \end{bmatrix} = \begin{bmatrix} h[1] & \dot{h}[1] & 1 \\ \vdots & \vdots & \vdots \\ h[N] & \dot{h}[N] & 1 \end{bmatrix} \cdot \begin{bmatrix} A \\ A\tau \\ ped \end{bmatrix} + \begin{bmatrix} w[1] \\ \vdots \\ w[N] \end{bmatrix} \tag{3}$$

where $y[n]$ is the nth time sample of the calorimeter readout signal, A is the pulse amplitude, $h[n]$ is the nth normalized reference pulse time sample, $\dot{h}[n]$ is the time derivative of $h[n]$, $w[n]$ is the nth time sample of the electronic noise, τ is the phase shift, which is linearized through a first-order Taylor expansion, and ped is a constant offset representing the pedestal base-line. Therefore, (3) is a particular implementation of (1) for calorimeter readout signals.

Equation (3) states that, knowing the calorimeter reference pulse shape and its derivative, the signal amplitude A can be determined together with the phase shift and the base line, using (2). In some calorimeters, the pedestal values are computed either through calibration runs or using pre-pulse samples and can be suppressed from (3). Similarly, the phase shift is ignored in some detectors as well. In any case, the $\mathbf{C}$ matrix should absorb the pile-up information for the current luminosity, in order to minimize its contribution on the parameter estimation error.

III. Source Recovery Through Deconvolution

For the proposed method, the digitized calorimeter electronic pulse information is interpreted as the output $y[n]$, where n is the time sample, of a linear time invariant (LTI) discrete-time system [18] whose impulse response is $h[n]$, as shown in Fig. 1. The sampled energy from a given collision event ($a[n]$ in Fig. 1) is modeled as an impulse signal, which represents the deposited energy in a calorimeter cell for the nth time sample or collision

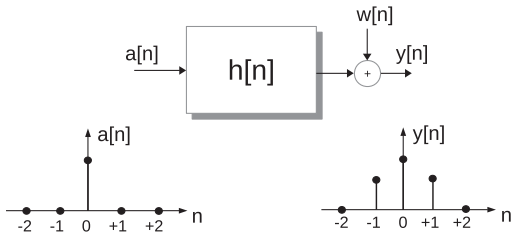

Fig. 1. LTI system model for calorimeter digitized data. $a[n]$ models the deposited energy in a given BC, $h[n]$ is the system impulse response, $y[n]$ is the actual acquired values, and $w[n]$ is the additive noise.

(BC). Thus, the LTI system output ($y[n]$) may be modeled as a shaped signal (the LTI impulse response), covering several adjacent BCs, plus electronic noise $w[n]$, which is assumed to be an independent and identically distributed Gaussian random process (White-Gaussian - WG).

In high-luminosity conditions, the BC occupancy at the system input is very high, resulting in signal superposition at the output. Calorimeter response can be modeled as the convolution between the input signal and the LTI system impulse response [18]

$$y[n] = \sum_i (h[i]a[n-i]) + w[n] \tag{4}$$

where the calorimeter impulse response $h[n]$ is equal to its reference pulse shape. Thus, in order to recover the input signal components, linear deconvolution techniques may be applied.

In case of free-running scenarios, one can recover the input signal by applying a causal version of an inverse filter with frequency response $1/H(z)$ (in case it is stable), where $H(z)$ is the complex frequency response of the LTI system [19], or, in other words, the Z-transform of the system impulse response $h[n]$. In the current application though, the trigger systems are capable of storing only a window containing the BC of interest and a few neighboring BCs. Consequently, the output information is partially available, and the input components cannot be fully recovered by applying an inverse filter.

For the case where the reference pulse shape extends to D bunch-crossings and N samples of $y[n]$ are stored, (4) can be better described in a compact vectorial form as follows:

$$\mathbf{y}_{N\times 1} = \mathbf{H}_{N\times P}\mathbf{a}_{P\times 1} + \mathbf{w}_{N\times 1} \tag{5}$$

where $P = D + N - 1$. In (5), $\mathbf{y}_{N\times 1}$ is the calorimeter output signal vector, $\mathbf{H}_{N\times P}$ is a matrix with P shifted versions of the calorimeter reference pulse, $\mathbf{a}_{P\times 1}$ is the calorimeter input signal vector (deposited energy in each BC), and $\mathbf{w}_{N\times 1}$ is the noise random vector. The vector and matrix dimensions are explicitly shown here, in order to clarify the underdeterminated characteristics of this system of equations.

Therefore, the system described in (5) does not have a unique solution for a given $\mathbf{a}$, since there are only N equations for P variables ($P > N$). The next section presents some modifications in order to produce a practical version of (5).

IV. Deconvolution Matrix

The proposed implementation consists of recovering only $p \leq N$ components of vector $\mathbf{a}$ in (5). The other signal components are absorbed by the new noise vector $\mathbf{w}_p$. Hence, the amplitude of the p central signals must be estimated simultaneously and the $\mathbf{w}_p$ noise vector includes electronic noise plus pile up from the remaining BCs. Equation (5) then becomes

$$\mathbf{y} = \mathbf{H}_p\mathbf{a}_p + \mathbf{w}_p \tag{6}$$

where the $\mathbf{H}_p$ is a $N \times p$ matrix comprising p shifted versions of the calorimeter reference signals whose amplitudes $\mathbf{a}_p$ must be determined. The procedure results in finding the $\mathbf{G}_p$ matrix, which is a $N \times p$ matrix that estimates the p input components $\hat{\mathbf{a}}_p$. Using the BLUE criterion again, the vector estimation equation is

$$\hat{\mathbf{a}}_p = \mathbf{G}_p'\mathbf{y}. \tag{7}$$

For unbiased estimators, it is required that

$$E\{\hat{\mathbf{a}}_p\} = \mathbf{G}_p'E\{\mathbf{y}\} = \mathbf{a}_p \tag{8}$$

where $E\{\cdot\}$ is the expected value of a random variable. Providing that the pedestal is removed from the noise as a preprocessing step and vector $\mathbf{w}_p$ is zero-mean, the expected value of $\mathbf{y}$ becomes

$$E\{\mathbf{y}\} = E\{\mathbf{H}_p\mathbf{a}_p + \mathbf{w}_p\} = \mathbf{H}_p\mathbf{a}_p. \tag{9}$$

Substituting (9) into (8) yields

$$\mathbf{G}_p'\mathbf{H}_p = \mathbf{I}_p. \tag{10}$$

The variances of the p estimators in $\mathbf{G}_p$ must be minimized by following the constraints given by (10). The procedure of simultaneous equations minimization with constraints can be found in [12] and it will lead to the vectorial BLUE closed formula

$$\mathbf{G}_p = \mathbf{C}_p^{-1}\mathbf{H}_p(\mathbf{H}_p'\mathbf{C}_p^{-1}\mathbf{H}_p)^{-1} \tag{11}$$

where $\mathbf{C}_p$ is the $N \times N$ covariance matrix of the noise vector $\mathbf{w}_p$. Therefore, the $\mathbf{C}_p$ matrix should absorb the second-order statistics of the shifted signals not included in $\mathbf{H}_p$.

Equation (11) performs the approximation of the deconvolution process for the $p \leq N$ selected components. The estimator designs for $p = 1$ and $p = N$ present special properties, which will be outlined next.

A. Estimator Design for the Central Signal Only

In this case, $p = 1$ and the $\mathbf{H}_1$ matrix reduces to the calorimeter reference pulse-shape vector $\mathbf{h}$. The noise covariance matrix should absorb the complete pile-up information, such as the optimal estimators presented in Section II. Thus, (11) becomes

$$\mathbf{G}_1 = \frac{\mathbf{C}^{-1}\mathbf{h}}{\mathbf{h}'\mathbf{C}^{-1}\mathbf{h}} \tag{12}$$

which is the amplitude estimator of the model given by (3), when the pedestal is removed as preprocessing and the signal phase shift is ignored [11].

Equation (12) is used for recovering the amplitude of the central BCID only, which is the one with relevant information according to the trigger system. For $p = 1$, (10) presents the minimal number of constraints. Thus, this estimator is expected to

exhibit the smallest variance among the linear estimators and, for Gaussian noise, it is known to be optimal as well (it is the minimal variance unbiased (MVU) estimator [12]). However, this estimator needs prior information about the pile-up statistics, since the noise covariance matrix contains information from all BCs.

The higher the values of p, the lower is the luminosity information absorbed by the noise covariance matrix $\mathbf{C}_p$, and the amplitude estimator vector becomes resilient to luminosity changes.

B. Estimator Design for the N Central Signals

Now, the case where $p = N$ will be considered, which is the best approximation of the complete deconvolution process. For the sake of simplicity, p will be omitted on the following equations. Such implementation consists of recovering the N central components of the vector $\mathbf{a}$ in (6).

Replacing (11) in (7), the BLUE estimator for the vector parameter $\mathbf{a}$ is

$$\hat{\mathbf{a}} = (\mathbf{H}'\mathbf{C}^{-1}\mathbf{H})^{-1}\mathbf{H}'\mathbf{C}^{-1}\mathbf{y} \tag{13}$$

where $\mathbf{H}$ is now a $N \times N$ matrix, $\mathbf{C}$ is the $N \times N$ noise covariance matrix, and $\mathbf{y}$ is the $N \times 1$ observed vector.

When the whole pulse is within the acquisition window ($D \leq N$), the pile-up information present in the $\mathbf{C}$ matrix is negligible (for $p = N$) for practical considerations. Therefore, the background comprises only the usual electronic noise, which is normally modeled as a WG process. As a result, the $\mathbf{C}$ matrix can be suppressed from (13), which can be extremely simplified as

$$\hat{\mathbf{a}} = \mathbf{H}^{-1}\mathbf{y}. \tag{14}$$

Although the estimator in (14) is a good approximation for the vectorial BLUE (for narrow signals), it is better understood as the minimal mean square error (MMSE) estimator, since the noise second-order statistics is not taken into account. The $\mathbf{H}^{-1}$ matrix is called the deconvolution matrix (DM) and it is computed offline for each calorimeter cell, since it needs the reference pulse-shape information only (the channel impulse response). The same matrix operation is applied for any nominal luminosity.

According to the constraints given by (10), an important property of $\mathbf{G}_p$ is that its ith estimator $\mathbf{g}_i$ is orthogonal to the reference signal $\mathbf{h}_j$ centered at the jth BC

$$\mathbf{g}_i'\mathbf{h}_j = \delta_{ij} \tag{15}$$

where δ_{ij} is the Kronecker delta. This orthogonality condition reflects the pile-up noise immunity of the method, emphasizing its luminosity-independent performance characteristics.

V. Simulation Results

In order to evaluate the performance of the proposed method, a unipolar pulse was used as a reference pulse shape from the electronics front end, and the pulse was considered to be fully within the acquisition window. Two different simulation scenarios were tested. The first one aims at quantifying the performance of the proposed method in a multiamplitude estimator point of view. The second simulation was built for evaluating the DM efficiency in a more realistic pile-up noise environment. It is also worth mentioning that the simulations use 64-b floating-point numbers and no quantization issues are taken into account.

TABLE I
NSDE and NRMSE (in %) with Respect to True Amplitude for Different Estimators, Where a_i is the Corresponding Estimation for the DM Method. Both BLUE 1 (B1) and BLUE 2 (B2) Provide Estimations Only for the Central BC

	B1	B2	a_{-3}	a_{-2}	a_{-1}	a_0	a_{+1}	a_{+2}	a_{+3}
NSDE	11.4	7.76	4.84	7.46	8.29	8.45	8.16	7.18	4.86
NRMSE	30.5	8.75	4.84	7.46	8.29	8.45	8.16	7.18	4.86

A. Performance Evaluation of DM for Amplitude Estimation

The simulation data set comprises 100 000 windows, and a symmetric pulse with a Gaussian-like shape in a window of 7 samples was considered. Pulses are generated simultaneously for all bunches within the window, considering the energy deposited in each bunch as a uniform distribution from 0 up to 600 MeV [15], [20], [21]. A WG noise with $\sigma = 20$ MeV is added to each window, reproducing typical electronic noise behavior in readout channels [22]–[24]. In this simulation, neither phase shift nor pulse deformation were taken into account. The data set was split into two sets of 50 000 events, one needed for designing the BLUE estimation methods, which are used here for comparison, and another used to evaluate the performance of the estimation methods.

Table I shows the normalized standard deviation error (NSDE) and the normalized root mean square error (NRMSE) between the true values and the estimates [see (16) and (17), respectively]

$$\text{NSDE} = \frac{\sqrt{\frac{\sum_{i=1}^{M}(e_i-\mu)^2}{M-1}}}{E_{\max}} \tag{16}$$

$$\text{NRMSE} = \frac{\sqrt{\frac{\sum_{i=1}^{M}e_i^2}{M}}}{E_{\max}}. \tag{17}$$

Here, μ is the mean value of the estimation error e (true energy minus estimated energy), and M is the total number of observations. Both formulas are normalized by the energy range E_{max} used in simulation. In order to compare with commonly used amplitude estimator methods, two signal models, based on (3), are employed. The method named here as BLUE 1 (B1) estimates the three parameters (A, τ, and ped) simultaneously, while the BLUE 2 (B2) method suppresses the base line and phase estimation, providing the estimator given by (12). The DM estimators are identified in Table I as a_i, with i indicating the time sample or the BCID, ranging from -3 to $+3$. These estimators exhibit a symmetrical error pattern with respect to the central BC due to the symmetry of the reference pulse-shape. This is due to the fact that in this simulation, since no signal outside the acquisition window is superimposed, the central signal is more difficult to deconvolve, presenting higher error.

Among the in-time estimators (BLUE 1, BLUE 2, and a_0), BLUE 2 presents the smallest NSDE and BLUE 1 is the worst case, showing that the constraint for pedestal immunity from

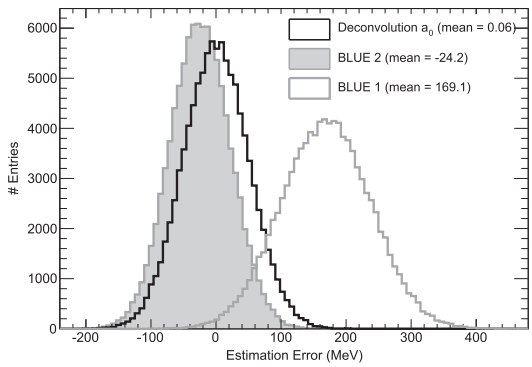

Fig. 2. Error distribution (truth estimation) for simulated pile-up noise, considering a_0, BLUE 1 and BLUE 2 estimators.

BLUE 1 is stronger than the six orthogonality constraints imposed by DM estimation. Different from the DM estimators, BLUE 2 and BLUE 1 present higher values for NRMSE than NSDE, indicating that these methods are biased in the presence of pile-up. This is expected, since they assume the presence of the in-time signal only, and do not have OOT signal orthogonality constraints. Despite BLUE 2 exhibiting the smallest NSDE among the in-time estimators, it requires an actual noise covariance matrix computation (the same for the BLUE 1 method), while no specific luminosity information is necessary for DM estimators.

Fig. 2 shows the error distribution for the three in-time methods, from which one can observe that the mean values (μ) for both BLUE 1 and BLUE 2 are different from zero. These bias values should be computed for each luminosity value and removed during event reconstruction, in order to avoid biased measurements under pile-up. It can also be concluded from this figure that the pedestal immunity constraint imposed by the BLUE 1 method becomes useless for non-Gaussian noise. The normalized kurtosis of -0.041 and -0.005 for BLUE 1 and BLUE 2, respectively, indicate that the noise is sub-Gaussian (excess negative kurtosis) [25] under pile-up and these methods are operating in suboptimal conditions. On the other hand, the noise presents stronger Gaussian features for DM (normalized kurtosis of 0.001), since only electronic noise is taken into account. Thus, DM estimators are operating on the Cramer-Rao limit [12] for multivariate Gaussian distribution and, therefore, they form an optimal vector estimator. It is worth mentioning that, due to the reduced number of constraints, BLUE 2 presents the best performance among the in-time estimators.

The Pearson correlation coefficients between the estimator outputs and true amplitude values are given in Table II. A_0 corresponds to the true amplitude for the in-time signals. Due to the orthogonality constraints (15), the cross-correlations among the seven DM components are very small and the signal superposition does not affect the DM estimators. The same behavior does not apply to both BLUE 1 and BLUE 2 methods. The higher cross-correlation factors degrade the performance of the BLUE 1 method significantly. This correlation is negative for any OOT signal, which agrees with the high positive bias presented in Fig. 2.

TABLE II
CORRELATION (IN %) BETWEEN TRUE AMPLITUDE A_i AND CORRESPONDING ESTIMATIONS, WHERE a_i IS THE CORRESPONDING ESTIMATION FOR THE DM METHOD. BOTH BLUE 1 AND BLUE 2 PROVIDE ESTIMATIONS ONLY FOR THE CENTRAL VALUE A_0

	A_{-3}	A_{-2}	A_{-1}	A_0	A_{+1}	A_{+2}	A_{+3}
BLUE 1	-14.4	-4.98	-3.68	**+93.1**	-4.18	-9.14	-12.0
BLUE 2	+1.67	-3.85	+5.71	**+96.6**	+5.75	-3.58	+1.62
a_{-3}	**+98.6**	-0.28	+0.26	+0.00	-0.08	-0.54	+0.28
a_{-2}	-0.05	**+96.8**	-0.40	+0.16	-0.52	-0.04	-0.23
a_{-1}	+0.23	-0.48	**+96.1**	-0.40	-0.14	-0.35	+0.38
a_0	-0.57	+0.68	-0.09	**+96.0**	+0.47	-0.19	-0.09
a_{+1}	+0.33	+0.14	+0.26	+0.17	**+96.3**	-0.40	-0.44
a_{+2}	-0.05	+0.24	-0.25	+0.31	+0.14	**+97.1**	-0.34
a_{+3}	+0.12	+0.16	+0.08	+0.15	-0.12	-0.34	**+98.6**

B. Performance Evaluation of DM in a High-Luminosity Collider Environment

A second data set was developed in order to evaluate the proposed method in a more realistic simulation of pile-up events in a collider experiment. Raw data with 1 000 000 time samples (BC), representing a sequence of ADC conversions from a given calorimeter readout channel, are populated randomly with a given occupancy factor (e.g., 10%).

For the nonempty BCs, an exponential distribution with $\mu =$ 80 MeV (mean value of the distribution) was used in order to emulate the energy deposition for the pile-up [20], [21], and reference pulse-shape signals (the same as described in Section V-A), with their respective amplitudes, are then superimposed. A random phase shift with a uniform distribution between $[-4, +4]\%$ was considered. In addition, a uniform random deviation between $[-1, +1]\%$ of the reference pulse value is applied, sample by sample, to each signal, in order to simulate small pulse deformations. After this step, a WG noise ($\sigma = 20$ MeV) is added to each sample, simulating the electronic noise. Finally, windows of seven samples (BC) were sequentially taken from the raw data.

Moreover, half of the data set is used for computing the weights for the optimal filter algorithms. The other half is used for analysis, in order to evaluate the performance of the considered estimation methods.

The reconstructed energy distributions, for an occupancy of 10%, are shown in Fig. 3. A logarithmic scale is employed in the vertical axis for better comparison between methods. The same shape is seen for all DM estimators, but only a_0 is shown for the sake of simplicity. BLUE 2 presents the best performance—sharpest negative tail and narrowest distribution around the origin. BLUE 1 exhibits a long left tail due to its high negative correlation with out-of-time signals. The right tails are similar, since they correspond to high amplitude in-time pile-up. These signals come from different events at the same BC. Hence, they are interpreted as regular in-time signals.

Fig. 4 shows the energy reconstruction for the three in-time estimators when no information from the luminosity is employed ($\mathbf{C} = \mathbf{I}$). The BLUE 1 estimator variance increases significantly, as can be seen from its higher negative tail. For BLUE 2, the main problem is due to the huge positive bias. Actually, after bias removal, the most probable value (MPV) from BLUE 2 distribution is -180 MeV, which is an undesirable reconstruction characteristics for final physics analysis.

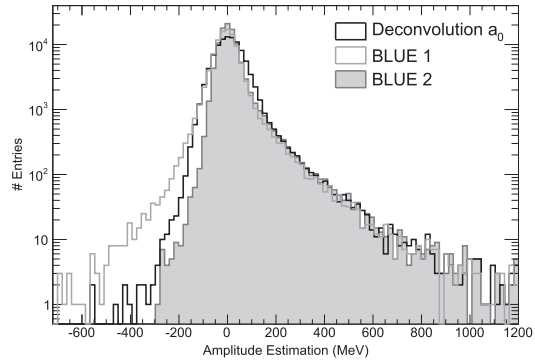

Fig. 3. Energy reconstruction for pile-up simulation. Actual luminosity information ($\mathbf{C}$) is used for the BLUE estimators.

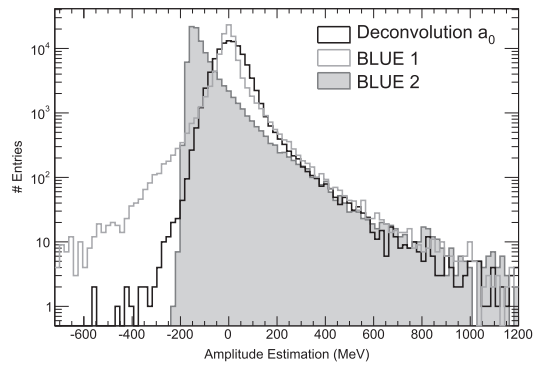

Fig. 4. Energy reconstruction for pile-up simulation. Actual luminosity information is not used for the BLUE estimators ($\mathbf{C} = \mathbf{I}$).

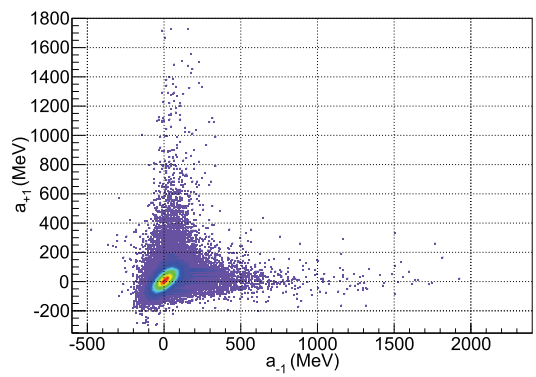

Fig. 5. Correlation between the DM estimators a_{-1} and a_{+1}. No correlation is observed above the noise due to the orthogonality of the DM estimators.

DM estimators remain the same, since they do not require any luminosity information.

Fig. 5 presents the correlation between a_{-1} and a_{+1} estimators. There is no correlation for signals above the noise, as expected. The same behavior is seen among all of the DM estimators, showing that there is no dependency among the energy deposited in different BCs, as expected.

The aforementioned analysis has shown that the deconvolution method recovers the amplitudes of adjacent signals with good accuracy and no luminosity-specific information is necessary. The amplitude information from adjacent BCs brings new perspectives for analysis and cuts that can be applied in order to increase the final energy reconstruction performance. The next section presents some suggestions for a procedure that can be used in high pile-up varying conditions.

VI. Combining Method

This section presents improvements that can be achieved when the optimality characteristic of BLUE 2 method is combined with the orthogonality constraint of DM. First, the improvement in the deconvolution performance itself is outlined. Second, it is shown how to use this approach to achieve better signal reconstruction fidelity. Finally, a comparison between the BLUE techniques and the proposed combining method is quantified in terms of estimation error. To this end, different front-end pulse-shapes operating under different conditions of occupancy and signal to pile-up ratio, are considered.

A. Multiamplitude Estimator

As shown in Section V, BLUE 2 presented better performance among the tested estimators, due to the reduced number of constraints and the absorption of the pile-up by the noise covariance matrix. However, there are some drawbacks (the same for BLUE 1):

- BLUE 2 design is luminosity dependent, since the noise covariance matrix will change with the pile-up level.
- The estimations are biased, since BLUE 2 weights are not explicitly orthogonal to OOT signals present in the event.
- The noise distribution becomes non-Gaussian under pile-up and BLUE 2 is no longer an optimal estimator design.

It was also shown that DM does not suffer from the problems listed before. However, due to the higher number of constraints, the performance of the DM estimators decreases in lower luminosity conditions. A tradeoff between both BLUE 2 and DM methods can be achieved by previously detecting the BC indices with significant pile-up incidence and forcing orthogonality only for those signals. This procedure minimizes the variance of the final estimator and allows an unbiased and luminosity-independent design.

The proposed scheme is shown in Fig. 6(a). Preprocessing for pile-up detection indicates the BCs where the superimposed signals are located in the observed window (if there is any). This information is used by the multiamplitude estimation (MAE) block, which performs the simultaneous estimation of the central signal together with the detected overlapped signals, imposing orthogonality to the detected OOT signals. Pile-up identification is obtained from DM, as shown in Fig. 6(b), where $\mathbf{H}^{-1}$ is the deconvolution matrix, as in (14). The amplitudes at the output of the deconvolution process are compared to a threshold computed by design. Those binary control signals feed the MAE block.

MAE is implemented using (11), for $p = K + 1$, where K is the number of detected OOT signals. Here, the $\mathbf{H}_p$ matrix contains the in-time reference pulse-shape signal plus the pulse shapes for the detected OOT signals. Since the pile-up is previously detected, the resulting vector parameter estimator works in optimal conditions (WG noise). In this case, (11) can be simplified to

$$\mathbf{G}_p = \mathbf{H}_p(\mathbf{H}_p'\mathbf{H}_p)^{-1} \tag{18}$$

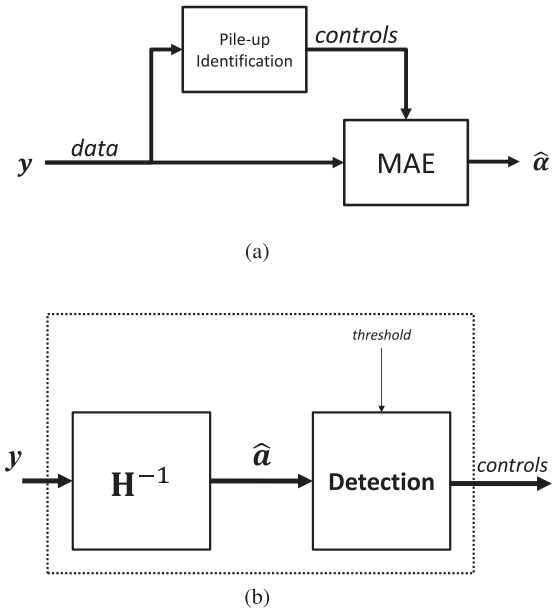

Fig. 6. Block diagrams for the proposed combined method (MAE) for energy estimation. (a) Overall diagram of the combined estimator method. The indices of the detected pile-up feed the MAE block. (b) Pile-up identification process using DM estimators. The detection is performed using a simple threshold set to be twice the rms noise.

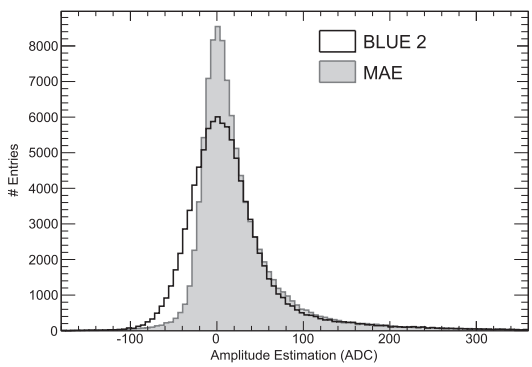

Fig. 7. Energy distribution for BLUE 2 and MAE methods.

which is a luminosity-independent vector amplitude estimator for the p signals. It can be noticed that $\mathbf{G}_p$, as given by (18), is the pseudoinverse [13] of $\mathbf{H}_p$, which is the MMSE solution of (10) for nonsquared convolution matrices. If no pile-up is detected, (18) becomes

$$\mathbf{G}_1 = \frac{\mathbf{h}}{\|\mathbf{h}\|^2}. \tag{19}$$

The estimator coefficients match the reference pulse shape, apart from reference signal energy normalization. The in-time estimator reaches the maximal performance on that configuration.

Fig. 7 shows the result when this combining approach is applied to the same simulation data as described in Section V-B. MAE presents a sharper negative tail, which leads to better energy resolution in final event reconstruction. The right tails are similar, since they come from in-time signals above the noise. In addition, while BLUE 2 uses the true covariance matrix for actual luminosity, no luminosity-dependent information is used in the combined method.

B. Signal Reconstruction Quality

The root mean square error (RMSE) between the recorded samples y_i and the reconstructed in-time pulse-shape is commonly used as a performance measure of the signal reconstruction [10], [16]. In absence of the phase estimation, it can be computed through

$$\mathrm{RE} = \sqrt{\sum_{i=1}^{N} \frac{(y_i - \hat{\alpha}_0 h_{0,i})^2}{N}} \tag{20}$$

where RE stands for the reconstruction error, y_i is the ith acquired time sample, $\hat{\alpha}_0$ is the estimated amplitude for the in-time signal, and $h_{0,i}$ is the ith time sample of the in-time reference pulse shape. Equation (20) shows accurate information for rejecting noisy and corrupted signal reconstructions in conditions where the signal shape is known to be invariant with the pulse amplitude. However, the RE value, as given by this equation, is expected to be higher for events with pile-up, even in the case of good in-time pulse amplitude estimations, being more suitable for pile-up detection in this case.

The dubious interpretation of (20) under pile-up conditions requires pursuing different procedures for estimation performance measures in high-luminosity scenarios. It turns out that both tasks can be performed using the MAE procedure proposed in Section VI-A. The pile-up identification procedure, presented in Fig. 6(b), points out the presence of significant OOT signals. Hence, the use of this procedure for pile-up detection is straightforward. In addition, unlike the RE threshold cut method, which only provides a global idea of the pile-up level, the proposed multiamplitude estimator also provides the BC index of each superimposed signal.

From the MAE outputs [see Fig. 6(a)], the amplitudes for the detected signals are estimated together with the in-time signal. This extra information can be used to improve the RE computation under pile-up, as follows:

$$\mathrm{RE}_{\mathrm{MAE}} = \sqrt{\sum_{i=1}^{N} \frac{\left(y_i - \hat{\alpha}_0 h_{0,i} - \sum_{j=1}^{K} \hat{\alpha}_j h_{j,i}\right)^2}{N}} \tag{21}$$

where j maps the BC indices for the K-detected OOT signals. The OOT signals are used as a correction to the final signal-shape reconstruction before the $\mathrm{RE}_{\mathrm{MAE}}$ computation, instead of being interpreted as noise. Therefore, $\mathrm{RE}_{\mathrm{MAE}} \approx \sqrt{\chi^2}$. Thus, the noise remains WG and the $\mathrm{RE}_{\mathrm{MAE}}$ still fits the likelihood probability. Hence, (21) becomes a good performance measure under pile-up conditions.

Fig. 8(a) and (b) shows the MAE in-time estimator versus the RE value, as computed from (20) (standard) and (21), respectively. Again, these analyses use the same simulation data as described in Section V-B. The signals for which pile-up was detected by the preprocessing method are in gray color. Fig. 8(a) shows that events with pile-up present higher RE values, when only the in-time signal is used on the signal reconstruction (20).

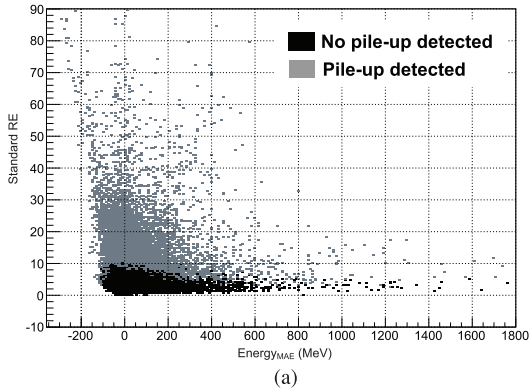

(a)

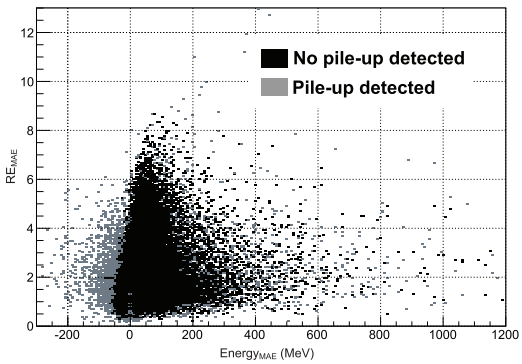

(b)

Fig. 8. Comparison between standard (RE) and proposed ($\mathrm{RE_{MAE}}$) reconstruction measures. (a) Standard RE error computation for MC simulation. (b) $\mathrm{RE_{MAE}}$ error using information from OOT signals.

This contrasts with Fig. 8(b), where the proposed $\mathrm{RE_{MAE}}$ computation is performed. Unlike (20), the proposed $\mathrm{RE_{MAE}}$, quantifies the performance of the energy reconstruction regardless of the reached pile-up level.

C. Performance for Different Calorimeter Responses

This section evaluates the performance of the MAE method for two different unipolar front-end pulses—one symmetric and other asymmetric. The symmetric pulse corresponds to the same one used previously, namely, a 7-sample window from a Gaussian-like shape that peaks at the fourth sample. As for the asymmetric pulse, the peak is located at the same position but exhibits a longer right tail, and requires 12 samples to be fully represented. For both cases, the entire pulse was considered to be within the acquisition window. This has often been the shaping strategy selected in modern calorimeters, as is the case for ALICE [7], D0 [5], ATLAS [6], and Zeus [4] experiments.

The simulation used to carry out this analysis is the same as described in Section V-B, where acquisition windows of W samples (BC) were sequentially taken from the raw data, being $W = 7$ and $W = 12$ for symmetric and asymmetric pulses, respectively. Half of the windows are used as a Noise set (electronic plus pile-up). Unlike the previous analysis, the other half is used to build the Signal set by adding a central signal (together with both phase-shift and deformation random distributions) to each window, corresponding to the target signal whose amplitude must be estimated. For these signals, the amplitude follows

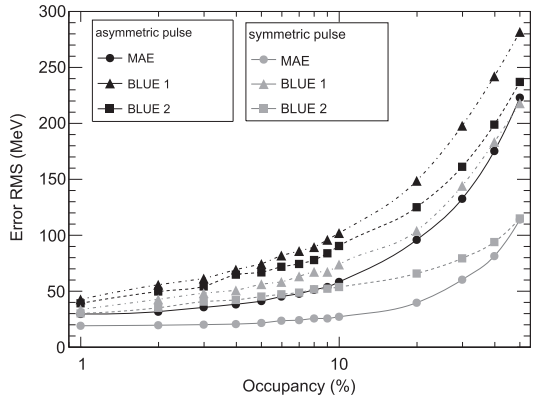

Fig. 9. Occupancy versus estimation error (rms) for the Signal set with a fixed SPR = 10 and considering symmetric (gray lines) and asymmetric (black lines) pulse shapes.

an exponential distribution with a given μ, corresponding to different signal-to-pile-up noise ratio (SPR). The SPR is computed according to the following equation:

$$\mathrm{SPR} = \frac{\mu_{\mathrm{signal}}}{\mu_{\mathrm{pile-up}}} \tag{22}$$

where μ_{signal} and $\mu_{\mathrm{pile-up}}$ are mean values of the exponential distribution of the signal and pile-up amplitudes in the simulation, respectively.

Fig. 9 shows the occupancy versus the estimation error for a fixed SPR of 10, when the Signal set is used (both pulse shapes were considered). From one side, 0% of occupancy means no pile-up (only electronic noise). On the other side, an occupancy of 50% means that, on average, there is energy deposition in the calorimeter channel of at least one of every two BCs. At very low occupancies, the pile-up is negligible and noise is approximately Gaussian. In this case, BLUE and MAE work close to the optimal design. For higher occupancies, MAE outperforms classic BLUE implementations. At very high occupancies (close to 50%), MAE and BLUE2 present similar results. However, no luminosity information is necessary for the MAE design. In addition, under such harsh conditions, signals outside the window start to contribute significantly and (14) is no longer valid. Concerning the different pulse shapes, the asymmetric pulse showed worse performance due to the long right tail which is more affected by the pile up, but it is worth mentioning that the MAE presented better performance for both pulses, as expected.

Regarding the estimation efficiency under different SPR conditions, Fig. 10 shows the result for a fixed occupancy of 10%. It can be seen that the higher the SPR level, the smaller is the estimation error for all considered methods. Once more, MAE outperforms the BLUE methods regardless of the pile-up noise level and pulse symmetry.

VII. Conclusions

This paper introduces a new concept in calorimeter energy estimation that can be applied to calorimeter design operating under pile-up conditions.

A luminosity-independent method for pulse amplitude estimation, which is based on calorimeter signal-shape DM, was introduced. Typically, only a few consecutive ADC samples are

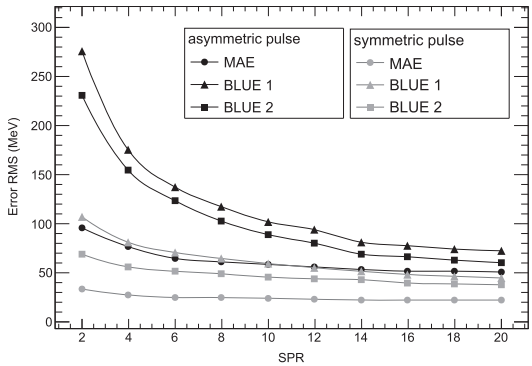

Fig. 10. SPR versus estimation error (rms) for the Signal set with a fixed occupancy of 10% and considering both symmetric (gray lines) and asymmetric (black lines) pulse shapes.

available and the complete deconvolution process is not feasible. However, the proposed optimal approximation based on MMSE presented good performance for the case where the reference pulse shape is within the readout window. It was shown that classical reconstruction algorithms, where the pedestal is previously suppressed and the phase shift is ignored, are particular solutions when a single amplitude estimation is performed. Due to the reduced number of constraints and providing that the pile-up noise is well characterized, this classical method achieves higher estimation performance. On the other hand, no pile-up noise characterization is necessary for DM, making it robust against luminosity variations. In addition, DM provides the amplitudes of the OOT signals as well.

In order to improve the final deconvolution performance, DM may be combined with the optimal characteristics of classical BLUE methods. Thus, an MAE method for high luminosity experiments is proposed. The MAE method enables fine tuning of the detected pulse amplitude estimation. The preprocessing procedure for pile-up detection enables constraint minimization and WG noise modeling, which leads to an optimal amplitude vector estimator design. It was shown that this vector estimator is the pseudoinverse of the convolution matrix for previously detected signals.

In addition to the optimal vector estimator design, the MAE method enables further investigations in higher-level event reconstruction procedures. As an example, a RE computation that is robust against out-of-time signals was proposed. With the proposed $\mathrm{RE}_{\mathrm{MAE}}$ computation, in-time event reconstruction may be correctly validated.

The MAE method presents higher computational cost, when compared to the FIR implementation of classical BLUE methods, since one matrix pseudoinverse operation must be performed. Therefore, further work is needed to implement this specific task using iterative methods, such as Conjugated Gradient, in order to implement MAE in modern field-programmable gate arrays for online reconstructions.

REFERENCES

[1] "LHC machine," in *JINST 3*, L. Evans and P. Bryant, Eds.. Bristol, U.K.: IOP, 2008, vol. S08001.
[2] R. R. Wilson, *The Tevatron*. Batavia, IL, USA: Fermilab FERMILAB-TM-0763, 1978.
[3] R. Wigmans, *Calorimetry - Energy Measurement in Particle Physics*. New York, USA: Oxford University Press, 2000.
[4] A. Caldwell *et al.*, "Design and implementation of a high precision readout system for the ZEUS calorimeter," *Nucl. Instrum. Meth. Phys. Res. A*, vol. 321, pp. 356–364, 1992.
[5] V. Abazov *et al.*, "The upgraded D0 detector," *Nucl. Instrum. Meth. Phys. Res. A*, vol. 565, pp. 463–537, 2006.
[6] M. Tylmad *et al.*, "Pulse shapes for signal reconstruction in the ATLAS tile calorimeter," in *Proc. IEEE NPSS Real Time Conf.*, 2009, pp. 543–547.
[7] H. Muller *et al.*, "Front-end electronics for PWO-based PHOS calorimeter of ALICE," *Nucl. Instrum. Meth. Phys. Res. A*, vol. 567, pp. 264–267, 2006.
[8] G. Bertuccio, E. Gatti, and M. Sapietro, "Sampling and optimum data processing of detector signals," *Nucl. Instrum. Meth. Phys. Res. A*, vol. 322, pp. 271–279, 1992.
[9] W. Cleland and E. G. Stern, "Signal processing considerations for liquid ionization calorimeters in a high rate environment," *Nucl. Instrum. Meth. Phys. Res. A*, vol. 338, pp. 467–497, 1994.
[10] E. Fullana *et al.*, "Digital signal reconstruction in the ATLAS hadronic tile calorimeter," *IEEE Trans. Nucl. Sci.*, vol. 53, no. 4, pp. 2139–2143, Aug. 2006.
[11] P. Adzic *et al.*, "Reconstruction of the signal amplitude of the CMS electromagnetic calorimeter," *Eur. Phys. J.*, vol. C46S1, pp. 26–35, 2006.
[12] S. M. Kay, *Fundamentals of Statistical Signal Processing, Estimation Theory*. Englewood Cliffs, NJ, USA: Prentice-Hall, 1993.
[13] S. O. Haykin, *Adaptive Filter Theory*, 4th ed. Upper Saddle River, NJ, USA: Prentice-Hall, 2001.
[14] H. Xu, Y. Chiu, and D. Gong, "A linear optimal filtering approach for pileup noise removal in high-rate liquid ionization calorimeters," presented at the Nucl. Sci Symp. Med. Imaging Conf., Seoul, Korea, 2013.
[15] M. Aleksa *et al.*, "ATLAS liquid argon calorimeter phase-i upgrade technical design report," vv ATLAS-TDR-022, CERN-LHCC-2013-017, 2013.
[16] M. Delmastro, "Quality factor analysis and optimization of digital filtering signal reconstruction for liquid ionization calorimeters," *Nucl. Instrum. Meth. Phys. Res. A*, vol. 600, pp. 545–554, 2009.
[17] C. Clement and P. Klimek, "Identification of pile-up using the quality factor of pulse shapes in the ATLAS tile calorimeter," in *Proc. IEEE Nucl. Sci Symp. Med. Imag. Conf.*, 2011, pp. 1188–1193.
[18] S. K. Mitra, *Digital Signal Processing: A Computer-Based Approach*, 3rd ed. New York, USA: McGraw-Hill, 2005.
[19] A. V. Oppenheim, *Discrete-Time Signal Processing*. Upper Saddle River, NJ, USA: Prentice-Hall, 2010.
[20] J. Chapman, "ATLAS simulation computing performance and pile-up simulation in ATLAS," presented at the LPCC Detector Simulation Workshop, Geneva, Switzerland, 2011.
[21] S. Banerjee *et al.*, "CMS simulation software," in *J. Phys.: Conf. Ser.*, 2012, vol. 396.
[22] C. Gabaldon, "Electronic calibration of the ATLAS LAr calorimeter and commissioning with cosmic muon signals," in *J. Phys.: Conf. Ser.*, 2009, vol. 160.
[23] G. Drake *et al.*, "The upgraded CDF front end electronics for calorimetry," *IEEE Trans. Nucl. Sci.*, vol. 39, no. 5, pp. 1281–1285, Oct. 2002.
[24] U. Behrens *et al.*, "Calibration of the forward and rear ZEUS calorimeter using cosmic ray muons," *Nucl. Instrum. Meth. Phys. Res. A*, vol. 339, no. 3, pp. 498–510, 1994.
[25] A. Hyvarinen, J. Karhunen, and E. Oja, *Independent Component Analysis*. Hoboken, NJ, USA: Wiley, 2001.